Anal Bioanal Chem (2003) 377 : 956–963
DOI 10.1007/s00216-003-2199-0

REVIEW

Martin Funovics · Ralph Weissleder · Ching-Hsuan Tung

Protease sensors for bioimaging

Received: 2 May 2003 / Revised: 3 July 2003 / Accepted: 31 July 2003 / Published online: 3 September 2003

Abstract Optical imaging of specific molecular targets and pathways in vivo has recently become possible through continued developments in imaging equipment, reconstruction algorithms, and more importantly the availability of imaging reporter molecules. These reporter molecules encompass photoproteins expressed in vivo and exogenously administered probes detectable by fluorescence and/or bioluminescence imaging. One particularly enticing aspect of optical imaging is the ability to design activatible probes with inherent amplification. This review summarizes our experience in developing novel near-infrared fluorescent (NIRF) imaging agents that report on protease activities. These agents are designed to be biocompatible, highly activatible, and able to produce bright NIRF following protease cleavage.

Keywords Optical Imaging · Neoplasms, detection · Fluorescence · Contrast agents, activatible

Introduction

Proteases play key roles in cardiovascular, oncologic, neurodegenerative, and inflammatory diseases. For example, proteases are thought to be crucial for invasion, metastasis, and angiogenesis in cancer [1]. Specifically, matrix metalloproteases (MMPs), cathepsins, and other types of proteases enable malignant cells to cross the basement membrane and digest extracellular matrix. Oncological treatments have been targeting these events; protease inhibitors currently represent a significant proportion of all newly developed drugs. In contrast, there has been a lack of in vivo non-invasive imaging techniques that could monitor specific protease activity. In this report, we describe the design of a series of newer activatible near infrared fluorescence (NIRF) imaging probes designed specifically for various proteases, and demonstrate their application in models of human disease. We believe that these agents, in addition to newly developed imaging technologies, will have far-reaching applications, both in animal models and in future clinical use regarding early diagnosis, drug discovery, and monitoring of treatment efficacies.

M. Funovics · R. Weissleder · C.-H. Tung (✉)
Center for Molecular Imaging Research, Harvard Medical School, Rm. 5406, 149 13th St., 02129 Charlestown, MA, USA
e-mail: tung@helix.mgh.harvard.edu

Optical Imaging

Optical imaging, which uses light at various wavelengths (UV to NIR) for image generation, includes many different acquisition techniques. Optical image contrast can be based on absorption, scattering, fluorescence, fluorescence lifetime, polarization [2], phase shifting [3], or reflection delay [4]. However, most meso- and macroscopic imaging is performed in the NIR region and based on either hemo/deoxyhemoglobin absorption [5], raman spectroscopy [6], or fluorescence. For fluorescence, the optimum wavelength for excitation and emission ranges from 650–900 nm [7]. Importantly, in this NIR window, tissues provides low absorption and low autofluorescence enabling higher signal-to-noise ratios (SNR).

A number of near infrared fluorochomes (excited at 650–900 nm) have previously been developed primarily for photographic applications, instrumentation [8], and more recently for DNA sequencing [9]. The ideal NIRF fluorochrome for in vivo imaging should have the following characteristics:

1. A peak fluorescence close to 700–900 nm
2. High quantum yield
3. Narrow excitation/emission spectrum
4. High chemical and photo-stability
5. Non-toxicity
6. Excellent biocompatibility, biodegradability, or excretability
7. Availability of monofunctional derivatives for conjugations
8. Commercial viability and production scalability for large quantities ultimately required for human use

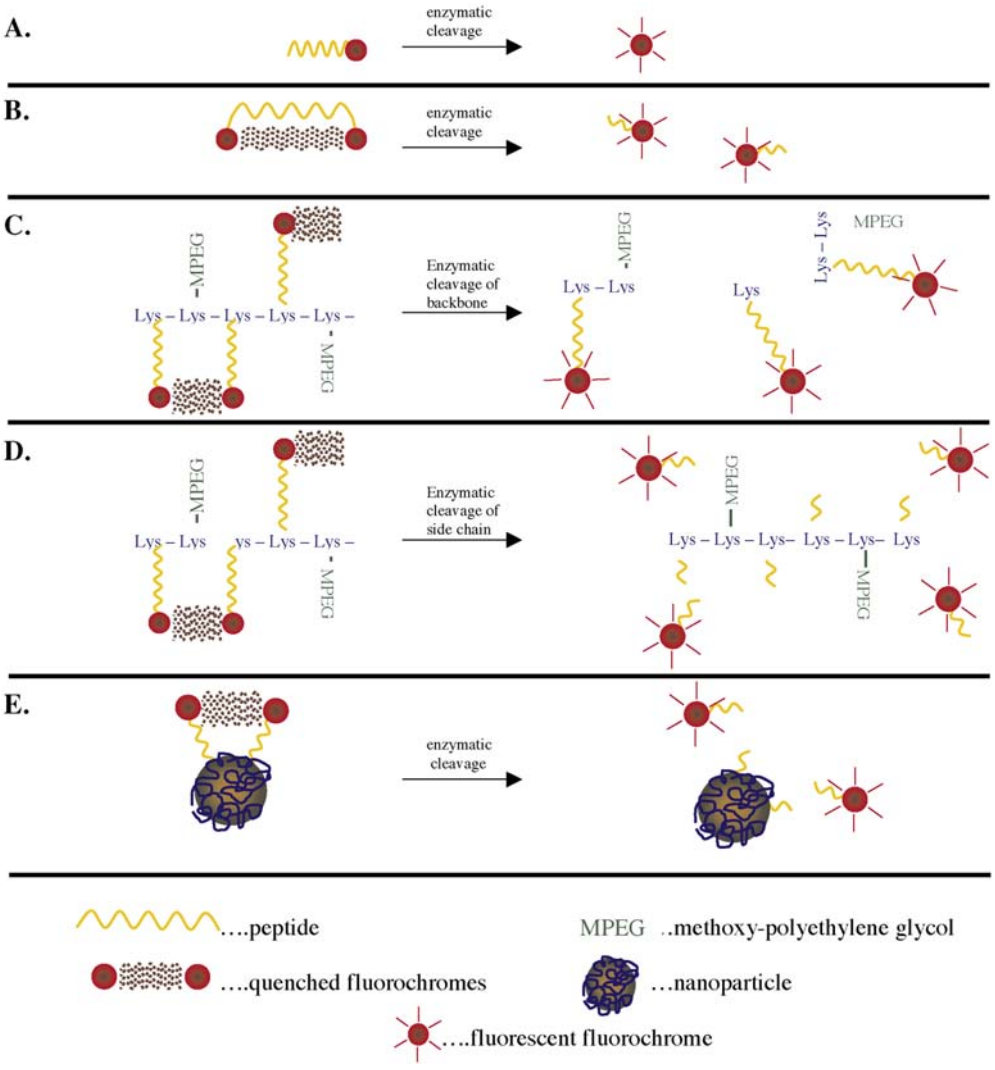

Fig. 1a–e Schematic structures of protease activatible probes. Fluorochromes are designed as protease substrate (**a**), covalently coupled to a protease substrate (**b**), to a polylysine backbone subjected to enzymatic cleavage (**c**), to a backbone sterically protected by methoxy-polyethylene-glycol (MPEG) via a synthetic peptide substrate (**d**), or to a nanoparticle (**e**). Due to the proximity of the fluorochromes, self-quenching occurs so that virtually no fluorescent signal can be detected in the non-activated states (*dotted lines*). After designated enzyme cleavage of the peptide spacer, fluorochromes are released from the carrier and brightly fluoresce

One substance which fits these specifications is indocyanine green (ICG) which is FDA approved for ophthalmic retinal angiography [10]. ICG has also been used as a compartmental contrast agent to facilitate breast cancer detection [11]and works similarly as other non-specific contrast agents used routinely for CT and MR imaging. ICG use in tens of thousands of patients showed lower side effects (<0.15%) compared to other contrast agents [12]. However, its use in designing targeted agents is primarily limited by the non-availability of monoderivatized activated precursors. Additional disadvantages of ICG are its hydrophobicity, relatively high albumin binding, nonlinear fluorescence and other intrinsic properties [13].

With the development of hydrophilic, monofunctional NIR fluorochromes, a variety of targeted (NIR fluorochrome attached to affinity ligands) and activatible imaging probes (based on a quenching–dequenching mechanism) have recently been developed. These probes have predominantly been used to detect early cancers or inflammatory processes in mouse models. In the future, however, many of these probes could be used in other disease models and/or as clinical imaging agents.

Protease activatible fluorescence probes

Different designs of protease-activatible NIR imaging probes are summarized in Fig. 1. In general, the principle mechanism of activation is based on quenching–dequenching upon protease cleavage. The NIR probes are typically designed to be maximally quenched in their native state and brightly fluorescent in their cleaved state. Ideally, the achieved signal amplification is up to several hundredfold. This approach of enzymatic activation of imaging agents has three major advantages over non-activatible imaging probes (e.g., radioisotope-based agents): (1) a single enzyme can cleave multiple fluorochromes, (2) reduced background because of quenching of the unactivated form, and (3) protease specificity by virtue of different substrates.

Internally activatible optical probes

Hydroxy- and amino-substituted coumarins have been the most widely used fluorophores for preparing fluorogenic

enzyme substrates [14]. Coumarin-based substrates produce highly soluble, intensely blue-fluorescent products (Fig. 1a). However, most of these dyes do not become fully fluorescent unless the pH of the reaction mixture is raised above pH 10. Thus, substrates derived from these fluorophores are seldom used for continuous measurement of enzymatic activity in solution or live cells. Newer derivatives of these dyes and newer chemical entities can be more compatible with physiologic environments, but have rarely been used in the NIR range [15].

Small molecule

Another approach in producing an enzyme-activatible sensor is to flank an enzyme substrate with two fluorophores or one fluorophore and a spectrally matched "quencher" molecule, which effectively absorbs the energy from the fluorophore via FRET without creation of fluorescence (Fig. 1b). For example, we have developed a non-fluorigenic NIR quencher for optimal energy transfer from NIR fluorescent probes. The chemical structure is based on an azulene dimer with a peak absorbance between 700 and 800 nm. It was coupled via a caspase-cleavable nonapeptide to a fluorophore (alexa 680). In the presence of caspase 3, a four-fold increase in fluorescent emission was observed [16].

The in vivo use of small molecule reporters is limited mainly by their unfavorable pharmacokinetics. A short plasma half-life and limited tissue penetration prevents the accumulation of sufficient concentrations of free fluorochrome in target tissues.

Large molecule, backbone cleavage

In order for the probe to reach its intended target enzyme, avoidance of rapid clearance and overcoming several structural barriers are important. These barriers include extravasation from vessels, diffusion through tissue, and cell membrane translocation in the case of targeting intracellular enzymes. To overcome these barriers, it was hypothesized that a long circulating, derivatizable polymer would represent one option for high tumoral delivery (Fig. 1c). We have utilized a polyethylene glycol protected graft co-polymer (PGC), previously developed for drug targeting [17], which consists of a poly-L-lysine backbone attached with multiple methoxy polyethylene glycol (MPEG) chains (Fig. 1c). These MPEG chains decrease the immunogenicity of the carrier, increase plasma half-life, and allow cell internalization of different payloads [18]. In mouse models, tumoral accumulation using this drug delivery system has been shown to be as high as 5–8% injected dose/g tumor. Plasma half-life in mice is about 24 h [19]. The free lysines on the partially unmodified backbone are available for protease (e.g., cathepsin B, trypsin) cleavage. This type of probe can be utilized in a number of biological applications (see below).

Large molecule, side chain cleavage

Introduction of cleavable linker molecules between the backbone and the fluorochromes in addition to complete substitution of the backbone amine groups with MPEG allows to achieve further protease specificity (Fig. 1d). A large number of protease-specific peptide substrates have been reported, the use of peptide libraries and phage display continues to produce newer substrates. In our experiments, ideal peptides are typically synthesized with a cysteine residue on the C-terminus for subsequent conjugation to the polylysine backbone. To prepare different NIRF probes, PGC is reacted with excess iodoacetyl anhydride to convert all available amino groups of the poly-L-lysine backbone into iodol groups. Enzyme specific substrate peptides are then attached to the iodoacetylated PGC through a thiol specific reaction. Following conjugation, NIR fluorochromes such as monoreactive Cy5.5 are attached to the *N*-terminus of the enzyme peptide substrate. Peptide and fluorochrome attachments are quantitated by individual absorption measurements. Typically 10–30 fluorochromes are attached to one PGC molecule. Enzyme selectivity is confirmed using enzymatic assays [20].

Nanoparticle-based cleavable agent

Nanoparticles are also used as a substrate for the attachment of fluorochromes (Fig. 1e), which provides two distinct advantages. First, conjugates made from superparamagnetic iron oxide particles can act both as a magnetic resonance and optical imaging contrast agent, thus enabling multimodality imaging. Second, different fluorochromes can be conjugated with different peptide spacers. This allows simultaneous multichannel assessment of several parameters (e.g., enzyme activities, perfusion, vascular permeability).

We have developed such a chimeric fluorescent/magnetic nanoparticle that provides both information on the anatomic location of the probe as a MRI contrast agent, and information on the molecular environment of the probe as an optical imaging agent [21]. MR contrast enhancement derives from superparamagnetic iron oxide core, the NIRF signal is generated by cleavable Cy5.5-derivatized peptides attached to amine groups on the nanoparticle surface. The peptide used to link the Cy5.5 with the iron oxide nanoparticle (RRRRGC) was attached to the amino groups on the surface of the nanoparticle. Between 1 and 2 peptide-Cy5.5 conjugates were attached to each CLIO particle. Upon cleavage of the spacer peptides by trypsin, the Cy5.5 fluorescence increased in vitro 12.8 fold [21].

NIRF Imaging technologies

The main imaging technologies currently available for detection of NIR probes are fluorescent reflectance imaging (FRI), fluorescent endoscopic imaging, fluorescence me-

diated tomography (FMT), and intravital fluorescence microscopy (i.e., epifluorescence, confocal, and multiphoton microscopy).

Fluorescent reflectance imaging

The simplest fluorescent reflectance imaging (FRI) system consists of a light source with the appropriate spectral intensities and an imaging camera with sufficient sensitivity in the NIR range. Optical bandpass filters are installed to avoid spectral overlap between the excitation and the emission wavelengths, so that only fluorescent light is captured by the camera [22]. First generation experimental systems were shown to have detection limits of NIR fluorochromes in the picomolar range, with target volumes around 1 μL. Second generation systems provided higher sensitivities and better resolution, and shorter acquisition times (<0.1 s). Most of the recent systems also possess multichannel capabilities, with simultaneous imaging of two or more dyes [23]. These systems could potentially allow real-time quantitative assessment of multiple enzyme activities. Another form of FRI are video rate intra-operative or other hand-held devices [24].

Fluorescent endoscopic imaging

Endoscopic systems are a subset of FRI systems, in which the excitation and emission light is applied through an endoscope. The feasibility and efficacy of fluorescence endoscopy has already been demonstrated in animal experiments as well as in human studies [25, 26]. Special imaging catheters have been designed to transmit NIR light and have also been miniaturized to submillimeter dimensions for endoscopic imaging in the mouse model [27]. One disadvantage of these systems, the limited aperture and thus energy flux through a fiberoptic bundle, can be potentially compensated by the close range to target.

Fluorescence mediated tomography

Fluorescence mediated tomography (FMT) is a tomographic imaging modality capable of quantitatively displaying deep NIRF signals in three-dimensional volume datasets [28]. Light is sent at the object in different consecutive directions and the corresponding emission photons that propagated through tissue are collected at multiple projections, quantitized, and then combined to obtain the distribution of fluorochromes in deep tissues [29]. The technique, similar in principle to diffraction tomography [30, 31], simultaneously uses absorption and fluorescent measurements for accurate 3-D reconstruction of fluorescent reporters [32]. Based on the raw emission and excitation data collected, a synthetic concentration–distribution model is constructed and applied to the inversion code for reconstructing absolute fluorochrome concentration in dense media [28, 33].

Recent measurements and modeling show that NIR fluorescent signals from tumor-like structures can propagate about 10 cm in breast or lung tissue and >5 cm in the adult brain [34]. Depth penetration may improve in the future with newer detection technologies, noise reduction, and utilization of more efficient beacons. An important advantage of FMT in respect to clinical tomographic imaging is its inherent quantitative nature.

Intravital microscopy

Intravital microscopy offers unsurpassed spatial resolution, however, its main limitation is depth penetration (approximately 50 μm for epifluorescent microscopy, 400 μm for confocal applications, and 800 μm for multi-photon microscopy). Intravital microscopy (IVM) has helped to provide powerful insights into gene expression and function in tumors, reveal the crucial role of host–tumor interactions in the biology of tumors and their responses to therapy, and indicated new approaches to improve cancer detection and treatment [35].

Direct access to the organ under investigation, typically through a surgical incision or window preparations [36], is necessary for intravital microscopy. In the epifluorescent application, a dichroic mirror in the microscope tube directs the excitation light through the objective onto the target while the fluorescent light enters the objective, is transmitted through the dichroic mirror, and propagates into the eyepiece or the imaging device.

A confocal microscope focuses a high-intensity laser beam through a high aperture objectives to a diffraction-limited spot in the specimen [37]. Fluorescent light is emitted from this spot, refocused by the objective, and projected onto a pinhole in the image plane. Only light from the focal plane of the objective can effectively pass through the pinhole as light originating from other planes will not be focused and unable to pass through the pinhole [38]. A confocal microscope records the intensity of a single pixel in the specimen at a time and acquires two-dimensional images as the laser beam is moved over the focal plane of the specimen. The focal plane can also be moved in the z direction to acquire three-dimensional datasets. The main advantage of confocal microscopy is the ability to produce an image of a distinct plane within the specimen rather than a summation image, as in epifluorescent microscopy [39].

Multi-photon microscopy uses the same laser scanning principle on the imaging side as confocal microscopy, but differs in its excitation mode. Multi-photon excitation [40] occurs as the result of simultaneous fluorophore absorption by either two or three photons in a single quantitized event. At high photon densities, the photons can be simultaneously absorbed (mediated by a virtual state) by combining their energies. By focusing and pulsing the excitation light source, the photon density necessary for excitation is achieved in a region of submicron size encompassing the microscope focal point [41], thus eliminating even further background fluorescence and out-of-focus flare

Table 1 Protease-activatible NIRF imaging probes currently under investigation, target proteases, and possible relevant diseases

Target protease	Disease	Substrate	Reference
Cathepsin B*	Cancer	K·K	[50]
PSA	Prostate cancer	HSSKLQ·	Unpublished
Cathepsin D	Breast cancer	PICF·F	[20]
MMP-2*	Metastases	PLG·VRG	[60]
HIV protease	HIV	GVSQNY·PIVG	Submitted data
HSV protease	HSV	LVLA·SSSFGY	Submitted data
Caspase-3*	Apoptosis	DEVD·	[16]
Caspase-1(ICE)	Apoptosis	WEHD·	Submitted data
Thrombin	Cardiovascular	F(Pip)R·S	[68]

*In development: MMP-1, MMP-7, MMP-9, MMP-13, Caspase-2, NFkB, Cathepsin S, K
K lysine, *H* histidine, *S* serine, *L* leucine, *Q* glycine, *P* proline, *I* isoleucine, *C* cystine, *F* phenylalanine, *V* valine, *A* alanine, *Y* tyrosine, *D* aspartate, *E* glutamine, *W* tryptophane, *Pip* pipeloic acid, *R* arginine, · cleavage site

that limit the effective sensitivity in conventional confocal microscopy, and obviating the need for a pinhole [42].

Examples of preclinical applications

Proteases play key roles in many pathophysiologic processes, such as degradation of extracellular matrix in arthritides, protease secretion in arteriosclerotic lesions, and activation of thrombin during the onset of thrombosis. The relative abundance of proteases in diseased tissues (even at early stages) makes them an attractive target both for imaging and for therapy [43, 44]. Table 1 illustrates examples of protease-specific NIRF probes that have been synthesized or are in development.

Imaging of cathepsins in tumors

Cathepsins are lysosomal proteases involved in cellular protein turnover and degradation [45, 46]. Cathepsin B, and D and S to a lesser extent, are overexpressed by a variety of malignant tumors, this making them potential candidates for tumor screening. In clinical studies, high tumoral cathepsin B expression has been associated with early tumor progression and poor survival [47]. The expression of cathepsin D has been found to be elevated 2–50 fold in breast cancers [48], and overexpression showed higher metastatic potential [49]. Specific probes both for cathepsin B [50] and D [20, 51] have been synthesized and tested in mouse tumor models with similar results. Tumors as small as 2 mm in the subcutaneous tissue, and intestinal adenomas as small as 50 µm could be imaged based on their cathepsin B expression [50].

Identification of colonic adenomatous polyps using a cathepsin B sensitive probe has been successfully achieved in a mouse model of colon cancer. These animals are heterozygous for a germ-line mutation in the mouse homolog of the human adenomatous polyposis coli (APC) gene ($APC^{Min/+}$ mouse (Fig. 2) [52]. The mice develop multiple small and large bowel adenomas, which simulate the dysplastic adenomatous polyps found in human disease [53]. Only after administration of the imaging probe, these lesions were highly conspicuous and even adenomas of sizes as small as 50 µm in diameter could be readily identified. Elevated cathepsin B expression correlated with the degree of cellular dysplasia in the polyps. This technique could have clinical use by allowing in vivo differentiation of small, highly dysplastic adenomas from innocuous lesions thus guiding selective removal.

Another use of the cathepsin B probe has been to test whether one can image varying expression levels of cathepsin B in tumors with different biological aggressiveness. Size- and depth-matched tumors from two mammarian carcinoma cell lines showing different levels of differentiation and protease expression were implanted in a nude mouse model and imaged after injection of activatible cathepsin B probe [54]. The results of this study showed that differing levels of protease activity in breast tumors can be measured by NIRF imaging. The highly aggressive DU4475 tumor revealed a significantly stronger NIRF signal in vivo compared with the well-differentiated BT20 lesion. The expression levels of cathepsin B protein correlated with the optical findings. In optical mammography, this imaging approach could thus potentially be used not only for tumor detection but also for molecular profiling of tumors for grading and differentiation.

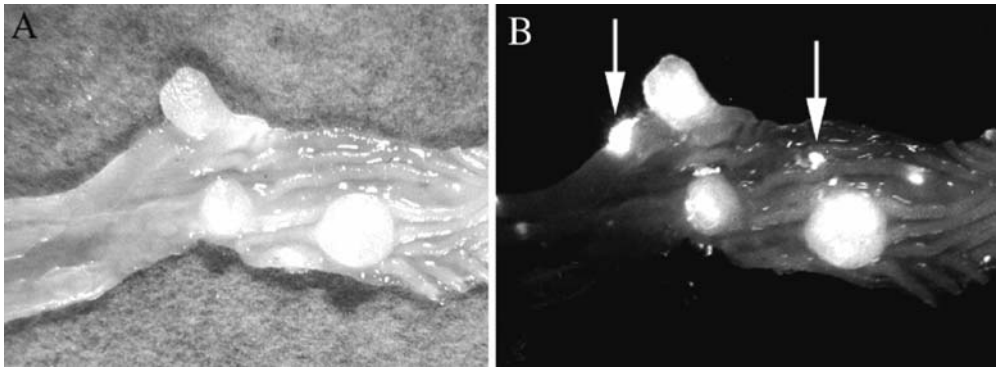

Fig. 2a, b Ex-vivo imaging of cathepsin B in dysplastic intestinal adenomas. Explanted mouse colon from APC^{min} mice with spontaneous adenomatous polyps after cathepsin-sensitive probe injection. **a** White light image showing large adenomas. **b** NIRF image, showing tumoral cathepsin activity as *white spots*, with additional smaller adenomas clearly visible (*arrows*). Reproduced with permission from [52]

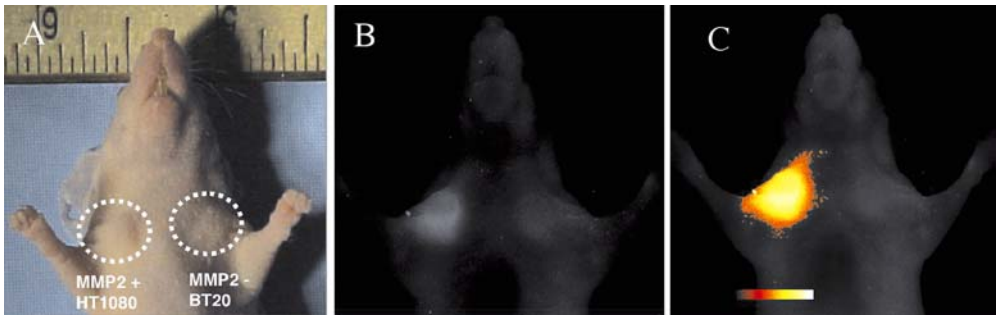

Fig. 3a–c Imaging of different expression levels of MMP-2, Nude mouse implanted with both an MMP-2 positive human HT1080 fibrosarcoma and an MMP-2 negative BT20 mammary adenocarcinoma. *Top*: Both tumors measured approximately 2–3 mm. **a** White light image showing the two tumors. **b** NIRF image 2 h after intravenous injection of the MMP-2-sensitive probe. The fibrosarcoma generates a strong fluorescent signal compared to the signal intensity of the BT20 tumor, which was only slightly above background. **c** Color-coded image. Reproduced with permission from [58]

Imaging expression and inhibition of matrix-metalloproteases

Several MMPs are overexpressed in cancers and the extent of expression has been shown to be related to tumor invasiveness, metastasis [55], and angiogenesis [56]. MMP-2 (gelatinase), being capable of degrading type-IV collagen, a major component of basement membranes [57], has been identified as a key MMPs in tumor biology. Based on these studies, different MMP inhibitors have been developed to treat malignant processes and even other diseases involving pathologic angiogenesis. In the course of preclinical and clinical testing of such inhibitors, there is a growing need for non-invasive methods to repeatedly assess the in vivo action of these inhibitors. For these reasons, an optical imaging probe activatible by MMP-2 has been synthesized. We have demonstrated the feasibility of imaging different activity levels of MMP (Fig. 3) [58]. An HT1080 human fibrosarcoma tumor model in the nude mouse was imaged both with and without the MMP-2 inhibitor, prinomastat. Treated animals showed significantly lower tumor fluorescence due to decreased MMP-2 activity [59, 60]. Utilization of MMP optical probes represents an approach for discerning the functional contributions of specific proteases in tumorigenesis and metastasis formation. In addition, it has also the ability to assess the efficacy of specific enzyme inhibitor treatment.

Arthritis

The cathepsin B probes have been tested in animal models of osteoarthritis and rheumatoid arthritis [61]. The probe was injected (2 nmol per animal), and images were taken

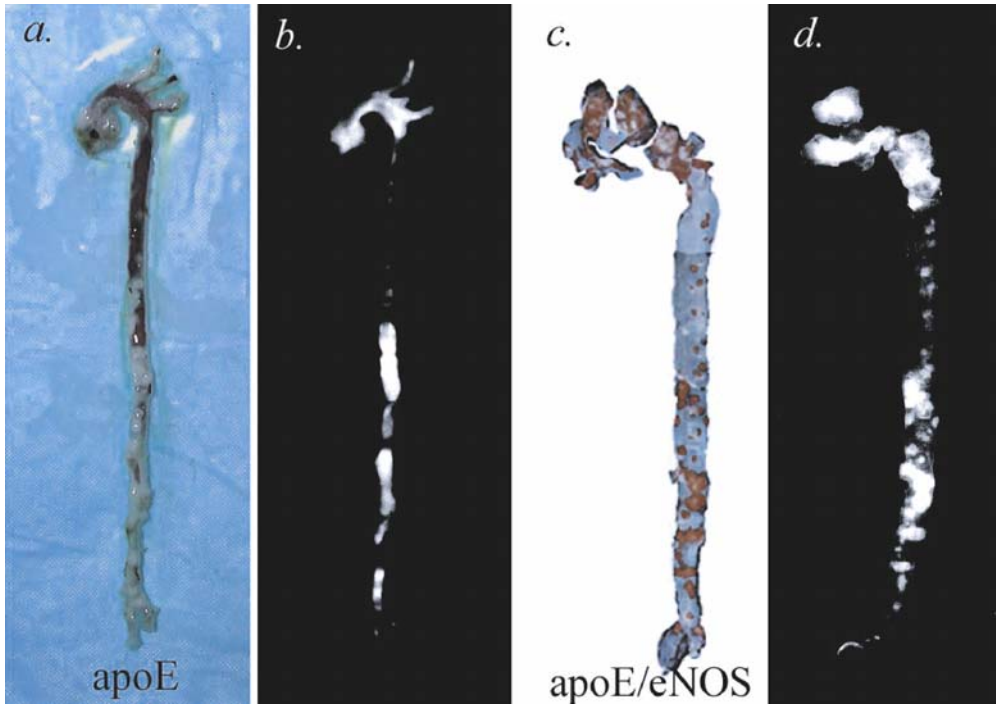

Fig. 4a–d Ex-vivo imaging of enzyme activity in aortic plaques. Aortas from apoE knockout mice fed a western type diet. **a** Unstained intact vessel with atherosclerotic lesions which appear white. **b** Corresponding NIRF image showing cathepsin B-activated fluorescent areas in the plaques. **c** Longitudinally opened aorta stained with Sudan IV. Lipid-rich areas appear red. **d** Corresponding NIRF image with prominent cathepsin B signal in the atherosclerotic lesions matching the Sudan staining. Reproduced with permission from [66]

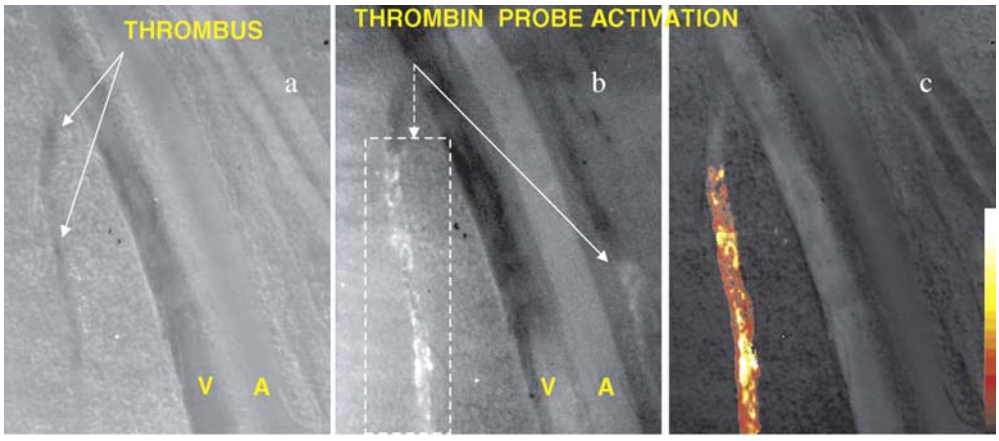

Fig. 5a–c Intravital microscopy of thrombin activity in thrombosis. **a** White light image of femoral vein in the mouse. After local application of $FeCl_3$, thrombosed segments of the vein are visible as darker areas (*arrows*). **b** NIRF image of the same area 90 min after thrombin-sensitive probe injection. Focal signal in areas of thrombosis, particularly within side branches (*arrows* and *dashed box*) are seen. **c** NIRF image superimposed onto the white light image demonstrating focal areas of high fluorescence signal within microthrombi. Reproduced with permission from [69]

24 h post injection. Specific probe cleavage by inflammatory cells secreting cathepsin resulted in increased fluorescence in the arthritic joints of the K/BxN mice. In contrast, the control wild-type animals showed no detectable fluorescence. More recent data indicate that cathepsin B imaging may also allow for monitoring the efficacy of disease therapy.

Atherosclerosis

In the US alone, vascular disease accounts for approximately one million deaths annually. Prevention and treatment of coronary artery disease (CAD) resulted in a 28.6% reduction in age-adjusted death rates between 1984 and 1994. However, CAD and ischemic stroke combined remain the primary killers in industrialized western countries and are of increasing prevalence in the rest of the world [62].

The first alteration of the arterial wall associated with atherosclerosis is a purely inflammatory lesion consisting of monocyte-derived macrophages and T lymphocytes. Monocytes invade the arteriosclerotic lesion (plaque), and proteases secreted by these and other cells may play a central role in different stages of atherogenesis. In particular, the resorption of the fibrous cap which leads to plaque instability and ultimately plaque rupture may center around protease activity. The ruptured plaque stimulates formation of thrombi, which may embolize, rapidly occlude the lumen and precipitate myocardial infarction or acute ischemic syndrome. There has been widespread interest in defining the characteristics underlying plaque rupture and subsequent thrombosis so that lesions with high risk for rupture can be identified for targeted interventions [63, 64].

Atherosclerotic lesions show high expression of different proteases (e.g., MMPs 1, 2, 8, 9, 13, cathepsins). Imaging of protease activity in atherosclerosis may serve as a new measure of plaque inflammation and vulnerability. ApoE knockout mice and apoE/endothelial NO synthetase (eNOS) double knockout mice were fed a western-type diet in order to promote arteriosclerosis [65]. The active plaques in these animals showed remarkable correlation between probe activation, and histological evidence of cathepsin B protease activity (Fig. 4) [66]. Such fluorescence imaging of enzyme activity in plaques, either with FMT or fiberoptic imaging catheters, can potentially be used in the fields of interventional radiology and vascular surgery in therapeutic management.

Thrombosis

One of the key enzymes in thrombus formation is thrombin, a serine esterase. Thrombin is also involved in tumor invasion, angiogenesis, and tissue injury [67]. Typically, detection of in vivo thrombin activity is achieved by assaying circulating thrombin-associated activation molecules in blood. Although these measurements provide evidence of systemic thrombin activity, local thrombin activity within normal and diseased tissues cannot be distinguished.

To image local thrombin activity in vivo, a specific human thrombin probe has been recently synthesized [68]. In experimental murine models with induced acute thrombosis of the femoral vein, thrombin activation of the probe resulted in focal NIRF signal enhancement in both occlusive and non-occlusive thrombi. Thrombin activity was also detected within acute and subacute thrombi and could be rapidly detected in vivo by fluorescence reflectance imaging systems (Fig. 5) [69]. Importantly, detection did not require injection of the probe prior to the event, but after formation of the thrombi at clinically relevant time points.

Using thrombin as a molecular target for thrombosis detection allows the preferential detection of biologically active thrombi (e.g., acute thrombi with high thrombin activity). This ability to distinguish biologically active thrombi is of substantial clinical importance, since fibrinolytic resistance markedly increases with thrombus age [70].

Acknowledgments Research summarized in this review was supported in part by NIH CA86355, CA88365, and NSF BES-0119382. M.A.F. was supported by a grant from the Max Kade Foundation, NY.

References

1. Kim J, Yu W, Kovalski K, Ossowski L (1998) Cell 94:353–62
2. Massoumian F, Juskaitis R, Neil MA, Wilson T (2003) J Microsc 209:13–22
3. van Munster EB, van Vliet LJ, Aten JA (1997) J Microsc 188: 149–57
4. Benaron DA, Ho DC, Spilman S, Van Houten JP, Stevenson DK (1994) Adv Exp Med Biol 361:207–14
5. Quaresima V, Matcher SJ, Ferrari M (1998) Photochem Photobiol 67:4–14.
6. Holtom GR, Thrall BD, Chin BY, Wiley HS, Colson SD (2001) Traffic 2:781–8
7. Weissleder R, Ntziachristos V (2003) Nat Med 9:123–8
8. McWhorter S, Soper S A (2000) Electrophoresis 21:1267–80
9. Steffens DL, Jang GY, Sutter SL, Brumbaugh JA, Middendorf LR, Muhlegger K, Mardis ER, Weinstock LA, Wilson RK (1995) Genome Res 5:393–9
10. Slakter JS, Yannuzzi LA, Guyer DR, Sorenson JA, Orlock DA (1995) Curr Opin Ophthalmol 6:25–32
11. Ntziachristos V, Yodh AG, Schnall M, Chance B (2000) Proc Natl Acad Sci USA 97:2767–72
12. Hope-Ross M, Yannuzzi LA, Gragoudas ES, Guyer DR, Slakter JS, Sorenson JA, Krupsky S, Orlock DA, Puliafito CA (1994) Ophthalmology 101:529–33
13. Mordon S, Devoisselle JM, Soulie-Begu S, Desmettre T (1998) Microvasc Res 55:146–52
14. Irvine GB, Ennis M, Williams CH (1990) Anal Biochem 185: 304–7
15. Sun WC, Gee KR, Haugland RP (1998) Bioorg Med Chem Lett 8:3107–10
16. Pham W, Weissleder R, Tung CH (2002) Angew Chem Int Ed Engl 4:3659–62
17. Bogdanov A, Weissleder R, Brady T (1995) Adv Drug Deliver Rev 16:335–348
18. Marecos E, Weissleder R, Bogdanov A Jr (1998) Bioconjug Chem 9:184–91
19. Weissleder R, Bogdanov A Jr, Tung CH, Weinmann HJ (2001) Bioconjugate Chem 12:213–9
20. Tung CH, Bredow S, Mahmood U, Weissleder R (1999) Bioconjugate Chem 10:892–6
21. Josephson L, Kircher MF, Mahmood U, Tang Y, Weissleder R (2002) Bioconjug Chem 13:554–60
22. Mahmood U, Tung CH, Bogdanov A Jr, Weissleder R (1999) Radiology 213:866–70
23. Mahmood U, Tung CH, Tang Y, Weissleder R (2002) Radiology 224:446–51
24. Nakayama A, del Monte F, Hajjar RJ, Frangioni JV (2002) Molecular Imaging 1:365–77
25. Messmann H, Endlicher E, Gelbmann CM, Scholmerich J (2002) Dig Liver Dis 34:754–61
26. Ito S, Muguruma N, Kusaka Y, Tadatsu M, Inayama K, Musashi Y, Yano M, Bando T, Honda H, Shimizu I, Ii K, Takesako K, Takeuchi H, Shibamura S (2001) Endoscopy 33:849–53
27. Manivasager V, Heng PW, Hao J, Zheng W, Soo KC, Olivo M (2002) Int J Oncol 21:1003–7
28. Ntziachristos V, Tung CH, Bremer C, Weissleder R (2002) Nat Med 8:757–60
29. Ntziachristos V, Chance B, Yodh AG (1999) Optics Express 5: 230–242
30. Arridge SR (1999) Inverse Problems 15:R41-R93
31. Paithankar DY, Chen AU, Pogue BW, Patterson MS, Sevick-Muraca EM (1997) Appl Opt 36:2260–2272
32. Ntziachristos V, Weissleder R (2001) Optics Lett 26:893–895
33. Ntziachristos V, Weissleder R (2002) Medical Phys 29:803–809
34. Ntziachristos V, Ripoll j, Weissleder R (2002) Optics Lett 27: 333–335
35. Jain RK, Munn LL, Fukumura D (2002) Nat Rev Cancer 2: 266–76
36. Petroll WM, Jester JV, Cavanagh HD (1996) Int Rev Exp Pathol 36:93–129
37. Callamaras N, Parker I (1999) Cell Calcium 26:271–9
38. Shuman H, Murray JM, DiLullo C (1989) Biotechniques 7:154–63
39. Parker I, Callamaras N, Wier WG (1997) Cell Calcium 21:441–52
40. Centonze VE (2002) Methods Cell Biol 70:129–48
41. Centonze VE, White JG (1998) Biophys J 75:2015–24
42. White N, Errington R (2002) Biotechniques 33:298–300, 302: 304–5
43. Wojtowicz-Praga SM, Dickson RB, Hawkins MJ (1997) Investigational New Drugs 15:61–75
44. Tamura Y, Watanabe F, Nakatani T, Yasui K, Fuji M, Komurasaki T, Tsuzuki H, Maekawa R, Yoshioka T, Kawada K, Sugita K, Ohtani M (1998) J Med Chem 41:640–9
45. Moin K, Demchik L, Mai J, Duessing J, Peters C, Sloane BF (2000) Adv Exp Med Biol 477:391–401
46. Reinheckel T, Deussing J, Roth W, Peters C (2001) Biol Chem 382:735–41
47. Maguire TM, Shering SG, Duggan CM, McDermott EW, O'Higgins NJ, Duffy MJ (1998) Int J Biol Markers 13:139–44
48. Escot C, Zhao Y, Puech C, Rochefort H (1996) Breast Cancer Res Treat 38:217–26
49. Garcia M, Platet N, Liaudet E, Laurent V, Derocq D, Brouillet J, Rochefort H (1995) Stem Cells 14:642–650
50. Weissleder R, Tung CH, Mahmood U, Bogdanov A Jr (1999) Nat Biotechnol 17:375–8
51. Tung CH, Mahmood U, Bredow S, Weissleder R (2000) Cancer Res 60:4953–8
52. Marten K, Bremer C, Khazaie K, Sameni M, Sloane B, Tung CH, Weissleder R (2002) Gastroenterology 122:406–14
53. Moser AR, Pitot HC, Dove WF (1990) Science 247:322–4
54. Bremer C, Tung CH, Bogdanov A, Jr, Weissleder R (2002) Radiology 222:814–8
55. Even-Ram S, Uziely B, Cohen P, Grisaru-Granovsky S, Maoz M, Ginzburg Y, Reich R, Vlodavsky I, Bar-Shavit R (1998) Nat Med 4:909–14
56. O'Reilly M S, Pirie-Shepherd S, Lane WS, Folkman J (1999) Science 285:1926–8
57. Karakiulakis G, Papanikolaou C, Jankovic SM, Aletras A, Papakonstantinou E, Vretou E, Mirtsou-Fidani V (1997) Invasion Metastasis 17:158–68
58. Bremer C, Bredow S, Mahmood U, Weissleder R, Tung CH (2001) Radiology 221:523–9
59. Bremer C, Tung CH, Weissleder R (2001) Nat Med 7:743–8
60. Bremer C, Tung CH, Weissleder R (2002) Acad Radiol 9 Suppl 2:S314–5
61. Ji H, Ohmura K, Mahmood U, Lee DM, Hofhuis F M, Boackle SA, Takahashi K, Holers VM, Walport M, Gerard C, Ezekowitz A, Carroll MC, Brenner M, Weissleder R, Verbeek JS, Duchatelle V, Degott C, Benoist C, Mathis D (2002) Immunity 16:157–68
62. Braunwald E (2001) Heart disease, 6th edn. WB Saunders, Philadelphia
63. Libby P (2001) The vascular biology of atherosclerosis. WB Saunders, Philadelphia
64. Naghavi M, Madjid M, Khan MR, Mohammadi RM, Willerson JT, Casscells SW (2001) Curr Atheroscler Rep 3:125–35
65. Nakashima Y, Plump AS, Raines EW, Breslow JL, Ross R (1994) Arterioscler Thromb 14:133–40
66. Chen J, Tung CH, Mahmood U, Ntziachristos V, Gyurko R, Fishman MC, Huang PL, Weissleder R (2002) Circulation 105:2766–71
67. Becker RC, Spencer FA (1998) J Thromb Thrombolysis 5: 215–229
68. Tung CH, Gerszten RE, Jaffer FA, Weissleder R (2002) ChemBioChem 3:207–211
69. Jaffer FA, Tung CH, Gerszten RE, Weissleder R (2002) Arterioscler Thromb Vasc Biol 22:1929–35
70. Robinson BR, Houng AK, Reed GL (2000) Circulation 102: 1151–7